H1prelim-17-071, ZEUS-prel-17-01
March 11, 2017
Draft version 3.0

Combination and QCD analysis of beauty and charm production cross section measurements in deep inelastic ep scattering at HERA

The H1 and ZEUS Collaborations

Abstract

Measurements of open beauty and charm production cross sections in deep inelastic *ep* scattering at HERA from the H1 and ZEUS Collaborations are combined. Reduced cross sections for beauty and charm production are obtained in the kinematic range of photon virtuality $2.5 \leq Q^2 \leq 2000$ GeV^2 and Bjorken scaling variable $3 \times 10^{-5} \leq x_{\mathrm{Bj}} \leq 5 \times 10^{-2}$. The combination method accounts for the correlations of the statistical and systematic uncertainties among the different data sets. The combined data are compared to perturbative QCD predictions and used together with the combined inclusive deep inelastic scattering cross sections from HERA to determine the charm and beauty quark masses.

1 Introduction

Measurements of open charm and beauty production in deep-inelastic electron[1]–proton scattering (DIS) at HERA provide important input for stringent tests of the theory of strong interactions, quantum chromodynamics (QCD). This note describes an extension of the previous H1 and ZEUS combination of charm measurements in DIS [1] with new charm and beauty data [2–8].

The primary aim of this analysis is to obtain a single consistent dataset which provides information on charm and beauty production in DIS in the full phase space, suitable for comparison with various theoretical predictions. The reduced charm and beauty cross-sections, $\sigma_{\rm red}^{c\bar{c}}$ and $\sigma_{\rm red}^{b\bar{b}}$, respectively, are combined to create one consistent set of charm and beauty cross-section measurements in the kinematic range of photon virtuality $2.5 \le Q^2 \le 2000$ GeV^2 and Bjorken scaling variable $3\times10^{-5} \le x_{\rm Bj} \le 5\times10^{-2}$ In this note, the combined data are compared to theoretical predictions obtained in the fixed-flavour-number scheme (FFNS) at next-to-leading order (NLO) QCD using HERAPDF2.0 and ABM11 proton distribution functions (PDFs) and approximate next-to-next-to-leading order (NNLO) using ABMP16 PDFs. The new combined data are used together with the combined inclusive deep inelastic scattering cross sections from HERA to determine the running charm and beauty quark masses in the QCD analysis at NLO.

2 Input data

The input data samples [2–14] used in the combination are listed in Tab. 1. Measurements have been obtained both from the HERA-I (1992–2000) and HERA-II (2003–2007) data-taking periods. The combination includes measurements of charm and beauty production performed using different tagging techniques: the reconstruction of particular decays of charmed mesons (datasets 2–7, 9, 10), the inclusive analysis of tracks exploiting lifetime information (datasets 1, 11) and the reconstruction of electrons and muons from heavy-flavour semi-leptonic decays (datasets 8, 12, 13).

Datasets 1–8 have been used in the previous combination [1], while datasets 9–13 are newly included. Note that dataset 9 replaces one of the datasets used in the previous combination [1] (dataset 8 from Table 1 of [1]), which is its subset. All cross sections are updated using the most recent hadron decay branching ratios [15].

3 Combination method

The quantities to be combined are the reduced charm and beauty cross sections, respectively, defined as:

$$\sigma_{\rm red}^{Q\bar{Q}} = \frac{{\rm d}^2\sigma^{Q\bar{Q}}}{{\rm d}x_{\rm Bj}{\rm d}Q^2}\cdot\frac{xQ^4}{2\pi\alpha^2\,(1+(1-y)^2)}. \quad (1)$$

[1]In this note, 'electron' is used to denote both electron and positron if not stated otherwise. For D mesons, charge-conjugate modes are implied.

Here $Q\bar{Q}$ stands for $c\bar{c}$ or $b\bar{b}$ quark-antiquark pairs, and y is the inelasticity. The cross section $\mathrm{d}^2\sigma^{Q\bar{Q}}/\mathrm{d}x_{\mathrm{Bj}}\mathrm{d}Q^2$ is given at the Born level without QED and electroweak radiative corrections, except for the running electromagnetic coupling α.

The combined cross sections are determined at common (x_{Bj}, Q^2) points. The grid points for $\sigma_{\mathrm{red}}^{c\bar{c}}$ are chosen to be the same as in [1], where 52 points were used, while for $\sigma_{\mathrm{red}}^{b\bar{b}}$ a subset of 27 of these points is used. The combined reduced cross sections are provided at the centre-of-mass energy $\sqrt{s} = 318$ GeV.

All measurements to be combined are already corrected to Born level (using running α). The results of the H1 inclusive lifetime analysis (dataset 1) are directly taken from the original measurement in the form of $\sigma_{\mathrm{red}}^{c\bar{c}}$ and $\sigma_{\mathrm{red}}^{b\bar{b}}$.[2] For all other measurements the inputs to the combination are visible cross sections, $\sigma_{\mathrm{vis,bin}}$, defined as the D-, μ-, e- or jet-production cross sections in a particular transverse momentun p_T and pseudorapidity η range, in bins of Q^2 and y or x_{Bj} . The reduced cross sections are obtained from $\sigma_{\mathrm{vis,bin}}$ using theoretical predictions:

$$\sigma_{\mathrm{red}}^{\mathrm{Q\bar{Q}}}(x_{\mathrm{Bj}}, Q^2) = \sigma_{\mathrm{vis,bin}} \frac{\sigma_{\mathrm{red}}^{\mathrm{Q\bar{Q},th}}(x_{\mathrm{Bj}}, Q^2)}{\sigma_{\mathrm{vis,bin}}^{\mathrm{th}}}. \tag{2}$$

To calculate the predicitons for the reduced cross sections $\sigma_{\mathrm{red}}^{\mathrm{Q\bar{Q},th}}(x_{\mathrm{Bj}}, Q^2)$ and visible cross sections $\sigma_{\mathrm{vis,bin}}^{\mathrm{th}}$, the theoretical calculations described in Section 4 are used. For charm production, they are consistent with those used in the previous combination [1].

The combination of reduced cross sections is based on the procedure described elsewhere and used in previous HERA combinations [1, 16–19], accounting for all correlations in the uncertainties. In the present analysis, the correlated and uncorrelated systematic uncertainties are predominantly of multiplicative nature, i.e. they change proportionally to the expected central values. The statistical uncertainties are mainly background dominated and thus are treated as constant. All experimental systematic uncertainties are treated as independent between H1 and ZEUS. For datasets 1, 8 and 11 statistical correlations between charm and beauty cross sections as reported in the original papers are accounted for. Where necessary the statistical correlation factors are corrected to take into account differences in the kinematic region of charm and beauty measurements (dataset 11) or binning schemes (dataset 1) using theoretical predictions. The consistent treatment of the correlations of statistical and systematic uncertainties, including the correlations between the charm and beauty data sets where relevant, yields a significant reduction of the overall uncertainties of the combined data.

4 Theoretical predictions

The cross-section predictions are obtained using the HVQDIS program [20] and the xFITTER (former HERAFITTER) framework [21] which provide NLO QCD ($O(\alpha_s^2)$) calculations in the 3-flavour FFNS for charm and beauty production in DIS. The predictions obtained with HVQDIS, which allows fully differential cross sections to be calculated, are used for phase-space corrections, while for the comparison to the combined data the predictions obtained with

[2] These measurements are transformed, when needed, to the common grid (x_{Bj}, Q^2) points using theoretical predictions, while the uncertainties on the resulting scaling factors are found to be negligible.

the xFITTER framework are used, which provides reduced cross-sections only, but has the advantage of using the running heavy-quark mass definition as implemented in the OPENQCDRAD program [22].

The following parameters are used in the calculations and are varied within the limits quoted below for estimating the uncertainties in the predictions introduced by these parameters:

- The **renormalisation and factorisation scales** are taken as $\mu_r = \mu_f = \sqrt{Q^2 + 4m_Q^2}$, where m_Q is the charm or beauty quark mass, respectively. The scales are varied simultaneously up or down by a factor of two.
- For the extrapolation to the full phase space, the **pole masses of the *c* and *b* quarks** are set to $m_c = 1.50 \pm 0.15$ GeV, $m_b = 4.50 \pm 0.25$ GeV, respectively. For the comparison with the combined data, the **running *c* and *b* quark masses** are set to the PDG values $m_c(m_c) = 1.27 \pm 0.03$ GeV, $m_b(m_b) = 4.18 \pm 0.03$ GeV [15]. These variations also affect the values of the renormalisation and factorisation scales.
- For the **strong coupling constant** the value $\alpha_s^{n_f=3}(M_Z) = 0.105 \pm 0.002$ is chosen which corresponds to $\alpha_s^{n_f=5}(M_Z) = 0.116 \pm 0.002$.
- The **proton PDFs** are described by a series of FFNS variants of the HERAPDF1.0 set [18] at NLO determined within the xFITTER framework. These proton PDFs are the same as those used in the previous combination [1]. In the determination of these PDF sets no charm measurements were included. For all parameter settings used here, the corresponding PDF set is used. In the extrapolation to the full phase space, an uncorrelated uncertainty of 2% is assigned to each extrapolated data point to cover the PDF uncertainties. As a cross check of the extrapolation procedure, the cross sections are also evaluated with the 3-flavour NLO versions of the HERAPDF2.0 set (FF3A) [19] and the differences are found to be well within the uncertainties quoted. For the comparison to the combined data the HERAPDF2.0 FF3A set [19] is used.

The NLO calculations performed with the HVQDIS program yield fully differential cross sections for charm and beauty quarks. For those cross-section measurements needing extrapolation factors from the visible phase space in which the measurements were performed to the reduced heavy-flavour cross sections, these predictions are extended with fragmentation models to provide hadron level cross sections. The fragmentation model for c quarks is based on the measurements by H1 [23] and ZEUS [24] as described in detail in [1]. The fragmentation model for b quarks uses the Peterson et al. [25] parametrisation with $\varepsilon_b = 0.0035 \pm 0.0020$ [26]. The fragmentation fractions of c quarks into specific charmed hadrons are taken from [27]. The branching fractions of semi-leptonic decays of heavy-quarks to a muon or electron are taken from [15] with the decay spectra of leptons modelled according to [28]. When necessary for the extrapolation procedure, the parton-level jets are reconstructed using the corresponding clustering algorithms, and the cross sections are corrected for jet hadronisation effects using corrections derived in the original papers [4, 6].[3]

[3] While no such corrections are provided in [6], an uncertainty of 5% is assigned to cover the missing hadronisation effects.

To evaluate the extrapolation uncertainty on the extracted reduced cross sections, all the above settings are varied by the corresponding uncertainties and each variation is considered as a correlated uncertainty among the measurements to which it applies, except for the uncertainties related to PDFs and hadronisation effects, which are treated as uncorrelated. Asymmetric variations are symmetrised using the largest deviations.

5 Combined data

In total, 209 charm and 57 beauty data points are combined simultaneously to 52 reduced charm and 27 beauty cross-section measurements, respectively. A total χ^2 of 149 for 187 degrees of freedom (dof) is obtained in the combination indicating consistency of input data and conservative estimates of the uncertainties. There are in total 167 sources of correlated uncertainties. These are 71 experimental systematic sources, 16 sources due to the extrapolation procedure (including the uncertainties on the fragmentation fractions and branching ratios) and 80 statistical charm and beauty correlations. None of these shifts exceeds 1.6 standard deviations. The pull distribution of the combination is shown in Fig. 1.

The individual datasets as well as the results of the combination are shown in Figs. 2 and 3. The combined data are significantly more precise than any of the individual input datasets. This is illustrated in Figs. 4 and 5 where the measurements for $Q^2 = 32$ GeV^2 are shown. Figs. 6 and 7 present a comparison of the NLO QCD predictions in the FFNS to the combined data. The theoretical uncertainties on these plots present the mass, scale and PDF[4] variations added in quadrature. The predictions describe the data reasonably well within the uncertainties in the whole kinematic range. Fig. 8 shows the combined reduced charm cross sections compared to the results of the previous combination [1] and theoretical predictions. This comparison demonstrates that the new combined charm data are also consistent with and slightly more precise than the previously published results.

6 QCD analysis

The combined beauty and charm data are included in a QCD analysis at NLO, together with the combined HERA inclusive DIS data [19].

6.1 Theoretical formalism and settings

The analysis is performed using an open-source QCD fit framework for PDF determination xFITTER [21] (version 1.2.0). The scale evolution of partons is calculated through DGLAP equations [29] at NLO, as implemented in the QCDNUM program [30] (version 17.01.11). The theoretical predictions for the HERA data are obtained using the OPENQCDRAD program [22] interfaced in the xFITTER framework. The number of active flavours is set to $n_f = 3$ at all scales. The renormalisation and factorisation scales for heavy-flavour production are set to

[4] Only experimental uncertainties ('EIG') of HERAPDF2.0 are considered.

$\mu_r = \mu_f = \sqrt{Q^2 + 4m_Q^2}$, where m_Q denotes the running mass of c or b quarks. The heavy-quark masses are left free in the fit if not stated otherwise. For the light-flavour contributions to the inclusive DIS cross sections, the pQCD scales are set to $\mu_r = \mu_f = Q$. The massless contribution to the longitudinal structure function F_L is calculated to $O(\alpha_s)$. The strong coupling strength is set to $\alpha_s^{n_f=3}(M_Z) = 0.106$. The Q^2 range of the inclusive HERA data is restricted to $Q^2 > Q^2_{\text{min}} = 3.5$ GeV^2. No such cut is applied to the charm and beauty data since $Q^2 + 4m^2$ is always > 3.5 GeV^2.

The χ^2 definition used for the HERA DIS data follows that of Eq. (32) in Ref. [19]. It includes an additional logarithmic term that is relevant when the estimated statistical and uncorrelated systematic uncertainties in the data are rescaled during the fit [31]. The correlated systematic uncertainties are treated through nuisance parameters.

The procedure for the determination of the PDFs follows the approach of HERAPDF2.0 [19]. The parametrized PDFs are the gluon distribution $xg(x)$, the valence quark distributions $xu_v(x)$ and $xd_v(x)$, and the u- and d-type antiquark distributions $x\overline{U}(x)$ and $x\overline{D}(x)$. At the initial QCD evolution scale $\mu^2_{\text{f0}} = 1.9$ GeV^2, the PDFs are parametrized as:

$$\begin{aligned}
xg(x) &= A_g x^{B_g}(1-x)^{C_g} - A'_g x^{B'_g}(1-x)^{C'_g}, \\
xu_v(x) &= A_{u_v} x^{B_{u_v}}(1-x)^{C_{u_v}}(1 + E_{u_v}x^2), \\
xd_v(x) &= A_{d_v} x^{B_{d_v}}(1-x)^{C_{d_v}}, \\
x\overline{U}(x) &= A_{\overline{U}} x^{B_{\overline{U}}}(1-x)^{C_{\overline{U}}}(1 + D_{\overline{U}}x), \\
x\overline{D}(x) &= A_{\overline{D}} x^{B_{\overline{D}}}(1-x)^{C_{\overline{D}}},
\end{aligned} \tag{3}$$

assuming the relations $x\overline{U}(x) = x\overline{u}(x)$ and $x\overline{D}(x) = x\overline{d}(x) + x\overline{s}(x)$. Here, $x\overline{u}(x)$, $x\overline{d}(x)$, and $x\overline{s}(x)$ are the up, down, and strange antiquark distributions, respectively. The sea quark distribution is defined as $\text{x}\Sigma(x) = x\overline{u}(x) + x\overline{d}(x) + x\overline{s}(x)$. The normalization parameters A_{u_v}, A_{d_v}, and A_g are determined by the QCD sum rules. The B and B' parameters determine the PDFs at small x, and the C parameters describe the shape of the distributions as $x \to 1$. The parameter C'_g is fixed to 25 [32]. Additional constraints $B_{\overline{U}} = B_{\overline{D}}$ and $A_{\overline{U}} = A_{\overline{D}}(1 - f_s)$ are imposed to ensure the same normalization for the xu and xd distributions as $x \to 0$. The strangeness fraction $f_s = xs/(xd + xs)$ is fixed to $f_s = 0.4$ as in the HERAPDF2.0 analysis [19].

The parameters in Eq. (3) are selected by first fitting with all D and E parameters set to zero, and then including them independently one at a time in the fit. The improvement in the χ^2 of the fit is monitored and the procedure is stopped when no further improvement is observed. This leads to the same 14 free PDF parameters, as in the inclusive HERAPDF2.0 analysis [19].

The PDF uncertainties are estimated according to the general approach of HERAPDF2.0 [19] in which the fit, model, and parametrization uncertainties are taken into account. Fit uncertainties are determined using the tolerance criterion of $\Delta\chi^2 = 1$. Model uncertainties arise from the variations of the strong coupling constant $\alpha_s^{n_f=3}(M_Z) = 0.106 \pm 0.0015$, the simultaneous variation of the factorisation and renormalisation scales up and down by a factor of two, the strangeness fraction $0.3 \leq f_s \leq 0.5$, and the value of $2.5 \leq Q^2_{\text{min}} \leq 5.0$ GeV^2 imposed on the HERA data. The parametrization uncertainty is estimated by extending the functional form in Eq. (3) of all parton distributions with additional parameters D and E added one at a time. An additional parametrisation uncertainty is considered by using the functional form in Eq. (3)

with $E_{u_v} = 0$, as the χ^2 in this variant of the fit is only 5 units worse than with the released E_{u_v} parameter. Furthermore, $\mu_{\rm f0}^2$ is varied within $1.6\ \mathrm{GeV}^2 < \mu_{\rm f0}^2 < 2.2\ \mathrm{GeV}^2$. The parametrization uncertainty is constructed as an envelope at each x value, built from the maximal differences between the PDFs resulting from the central fit and all parametrization variations. This uncertainty is valid in the x range covered by the PDF fit to the data. The total PDF uncertainty is obtained by adding the fit, model, and parametrization uncertainties in quadrature. In the following, the quoted uncertainties correspond to 68% CL.

6.2 Results

The results for the fitted heavy-quark masses extracted from the fit using the inclusive and combined beauty and charm data are:

$$
\begin{aligned}
m_c(m_c) &= 1290^{+46}_{-41}(\mathrm{fit})^{+62}_{-14}(\mathrm{mod})^{+7}_{-31}(\mathrm{par})\ \mathrm{MeV}, \\
m_b(m_b) &= 4049^{+104}_{-109}(\mathrm{fit})^{+90}_{-32}(\mathrm{mod})^{+1}_{-31}(\mathrm{par})\ \mathrm{MeV}.
\end{aligned}
\tag{4}
$$

The model uncertainties are dominated by theoretical uncertainties arising from the scale variations. The fit yields $\chi^2/\mathrm{dof} = 1435/1208$. The results obtained in the fit using the inclusive data only are: $m_c(m_c) = 1798^{+144}_{-134}(\mathrm{fit})$ MeV, $m_b(m_b) = 8450^{+2282}_{-1812}(\mathrm{fit})$ MeV (note that only the fit uncertainties are quoted). In the variant of the fit using the inclusive data only and the reduced parametrisation with $E_{u_v} = 0$ the central fitted values for the heavy-quark masses are: $m_c(m_c) = 1450$ MeV, $m_b(m_b) = 3995$ MeV.

A cross check is performed using the Monte Carlo method [33,34]. It is based on analysing a large number of pseudo data sets called replicas. For this cross check, 500 replicas are created by taking the combined data and fluctuating the values of the reduced cross sections randomly within their given statistical and systematic uncertainties taking into account correlations. All uncertainties are assumed to follow Gaussian distributions. The central values for the fitted parameters and their uncertainties are estimated using the mean and RMS values over the replicas. The obtained heavy-quark masses and their fit uncertainties are in agreement with those quoted in Eq. (4). We conclude that the inclusive data alone can not reliably constrain the quark masses, and that the systematics from including the inclusive data in the global mass fit are covered by the parametrisation uncertainties applied.

The predictions for the combined data are also calculated using the ABM11 PDFs [35] at NLO, and ABMP16 PDFs [36] at approximate NNLO as implemented in the OPENQCDRAD program interfaced in the XFITTER framework. They are compared to the combined data in Figs. 9 and 10. Both calculations yield very similar description of the data to the one obtained using HERAPDF2.0 FF3A, which is further illustrated by the comparisons where all results are normalised to the predictions obtained using HERAPDF2.0 FF3A (see Figs. 11 and 12). In order to quantify the level of agreement, the χ^2 values are calculated and reported in Table 2.

7 Summary

Measurements of beauty and charm production cross sections in deep-inelastic ep scattering by the H1 and ZEUS experiments were combined at the level of reduced cross sections, accounting for their statistical and systematic correlations. The beauty cross sections have been combined for the first time. The data sets were found to be consistent and the combined data have significantly reduced uncertainties. The combined data were compared to NLO QCD predictions, which are found to describe the data reasonably well. The running charm and beauty masses were extracted in the QCD analysis using the inclusive HERA DIS and new combined charm and beauty data.

References

[1] F. D. Aaron *et al.* [H1 and ZEUS Collaborations], "Combination and QCD Analysis of Charm Production Cross Section Measurements in Deep-Inelastic ep Scattering at HERA", Eur. Phys. J. **C73**, (2013) 2311 [arXiv:1211.1182].

[2] H. Abramowicz *et al.* [ZEUS Collaboration], "Measurement of $D^{\pm}$ Production in Deep Inelastic ep Scattering with the ZEUS detector at HERA", JHEP **05**, (2013) 023 [arXiv:1302.5058].

[3] H. Abramowicz *et al.* [ZEUS Collaboration], "Measurement of $D^{*\pm}$ Production in Deep Inelastic Scattering at HERA", JHEP **05**, (2013) 097 [arXiv:1303.6578]. Erratum-ibid JHEP **02**, (2014) 106.

[4] H. Abramowicz *et al.* [ZEUS Collaboration], "Measurement of beauty and charm production in deep inelastic scattering at HERA and measurement of the beauty-quark mass", JHEP **09**, (2014) 127 [arXiv:1405.6915].

[5] H. Abramowicz *et al.* [ZEUS Collaboration], "Measurement of beauty production in deep inelastic scattering at HERA using decays into electrons", Eur. Phys. J. **C71**, (2011) 1573 [arXiv:1101.3692].

[6] H. Abramowicz *et al.* [ZEUS Collaboration], "Measurement of beauty production in DIS and F2bb extraction at ZEUS", Eur. Phys. J. **C69**, (2010) 347 [arXiv:1005.3396].

[7] S. Chekanov *et al.* [ZEUS Collaboration], "Measurement of charm and beauty production in deep inelastic ep scattering from decays into muons at HERA", Eur. Phys. J. **C65**, (2010) 65 [arXiv:0904.3487].

[8] F. D. Aaron *et al.* [H1 Collaboration], "Measurement of the Charm and Beauty Structure Functions using the H1 Vertex Detector at HERA", Eur. Phys. J. **C65**, (2010) 89 [arXiv:0907.2643].

[9] A. Aktas *et al.* [H1 Collaboration], "Production of D*+- Mesons with Dijets in Deep-Inelastic Scattering at HERA", Eur. Phys. J. **C51**, (2007) 271 [hep-ex/0701023].

[10] F. D. Aaron *et al.* [H1 Collaboration], "Measurement of $D^{*\pm}$ Meson Production and Determination of F_2^{ccbar} at low Q2 in Deep-Inelastic" Eur. Phys. J. **C71**, (2011) 1769 [arXiv:1106.1028].

[11] F. D. Aaron *et al.* [H1 Collaboration], “Measurement of the D*+- Meson Production Cross Section and F(2)**(c c-bar), at High Q**2, in ep Scattering at HERA”, Phys. Lett. **B686**, (2010) 91 [arXiv:0911.3989].

[12] J. Breitweg *et al.* [ZEUS Collaboration], “Measurement of D*+- production and the charm contribution to F2 in deep inelastic scattering at HERA”, Eur. Phys. J. **C12**, (2000) 35 [hep-ex/9908012].

[13] S. Chekanov *et al.* [ZEUS Collaboration], “Measurement of D*+- production in deep inelastic e+- p scattering at HERA”, Phys. Rev. **D69**, (2004) 012004 [hep-ex/0308068].

[14] S. Chekanov *et al.* [ZEUS Collaboration], “Measurement of D+- and D0 production in deep inelastic scattering using a lifetime tag at HERA”, Eur. Phys. J. **C63**, (2009) 171 [arXiv:0812.3775].

[15] C. Patrignani *et al.* [Particle Data Group], “2016 Review of Particle Physics”, Chin. Phys. **C40**, (2016) 100001.

[16] A. Glazov, Proceedings of “13th International Workshop on Deep Inelastic Scattering”, eds. W. H. Smith and S. R. Dasu, Madison, USA, 2005, AIP Conf. Proc. **792**, (2005) 237.

[17] A. Atkas *et al.* [H1 Collaboration], “Measurement of the Inclusive ep Scattering Cross Section at Low Q^2 and x at HERA”, Eur. Phys. J. **C63**, (2009) 625 [arXiv:0904.0929].

[18] F. D. Aaron *et al.* [H1 and ZEUS Collaboration], “Combined Measurement and QCD Analysis of the Inclusive e+- p Scattering Cross Sections at HERA”, JHEP **01**, (2010) 109 [arXiv:0911.0884].

[19] H. Abramowicz *et al.* [H1 and ZEUS Collaborations], “Combination of measurements of inclusive deep inelastic $e^{\pm}p$ scattering cross sections and QCD analysis of HERA data”, Eur. Phys. J. **C75**, (2015) 580 [arXiv:1506.06042].

[20] B. W. Harris and J. Smith, “Charm quark and D*+- cross-sections in deeply inelastic scattering at HERA”, Phys. Rev. **D57**, (1998) 2806 [hep-ph/9706334].

[21] S. Alekhin *et al.*, “HERAFitter”, Eur. Phys. J. **C75**, (2015) 304 [arXiv:1410.4412], `www.xfitter.org`.

[22] S. Alekhin, J. Blümlein, S. Moch, “Parton Distribution Functions and Benchmark Cross Sections at NNLO”, Phys. Rev. D86 (2012) 054009, doi: 10.1103/PhysRevD.86.054009, [arXiv:1202.2281];

I. Bierenbaum, J. Blümlein, S. Klein, “The Gluonic Operator Matrix Elements at O(alpha(s)**2) for DIS Heavy Flavor Production”, Phys. Lett. B672 (2009) 401, doi: 10.1016/j.physletb.2009.01.057, [arXiv:0901.0669];

S. Alekhin, OPENQCDRAD-1.5. `http://www-zeuthen.desy.de/~alekhin/OPENQCDRAD`.

[23] F. D. Aaron *et al.* [H1 Collaboration], “Study of Charm Fragmentation into $D^{*\pm}$ Mesons in Deep-Inelastic Scattering at HERA”, Eur. Phys. J. **C59**, (2009) 589 [arXiv:0808.1003].

[24] S. Chekanov *et al.* [ZEUS Collaboration], “Measurement of the charm fragmentation function in D^* photoproduction at HERA”. JHEP **04**, (2009) 082 [arXiv:0901.1210].

[25] C. Peterson *et al.*, “Scaling Violations in Inclusive e+ e- Annihilation Spectra”, Phys. Rev. **D27**, (1983) 105.

[26] P. Nason and C. Oleari, “A Phenomenological study of heavy quark fragmentation functions in e^+e^- annihilation”, Nucl. Phys. **B565**, (2000) 245 [hep-ph/9903541].

[27] M. Lisovyi *et al.*, “Combined analysis of charm-quark fragmentation-fraction measurements”, Eur. Phys. J. **C76**, (2016) 397 [arXiv:1509.01061].

[28] N. E. Adam *et al.* [Cleo Collaboration], “Absolute Branching Fraction Measurements for D+ and D0 Inclusive Semileptonic Decays”, Phys. Rev. Lett. **97**, (2006) 251801 [hep-ex/0604044].

[29] Y. L. Dokshitzer, “Calculation of the Structure Functions for Deep Inelastic Scattering and e+ e- Annihilation by Perturbation Theory in Quantum Chromodynamics.,” Sov. Phys. JETP **46** (1977) 641 [Zh. Eksp. Teor. Fiz. **73** (1977) 1216].

V. N. Gribov and L. N. Lipatov, “Deep inelastic *ep* scattering in perturbation theory”, Sov. J. Nucl. Phys. 15 (1972) 438;

G. Altarelli and G. Parisi, “Asymptotic freedom in parton language”, Nucl. Phys. B126 (1977) 298, doi:10.1016/0550-3213(77)90384-4;

G. Curci, W. Furmanski, and R. Petronzio, “Evolution of parton densities beyond leading order: The non-singlet case”, Nucl. Phys. B175 (1980) 27, doi:10.1016/0550-3213(80)90003-6;

W. Furmanski and R. Petronzio, “Singlet parton densities beyond leading order”, Phys. Lett. B97 (1980) 437, doi:10.1016/0370-2693(80)90636-X;

S. Moch, J. A. M. Vermaseren, and A. Vogt, “The three-loop splitting functions in QCD: the non-singlet case”, Nucl. Phys. B688 (2004) 101, doi:10.1016/j.nuclphysb.2004.03.030, [arXiv:hep-ph/0403192];

A. Vogt, S. Moch, and J. A. M. Vermaseren, “The three-loop splitting functions in QCD: the singlet case”, Nucl. Phys. B691 (2004) 129, doi:10.1016/j.nuclphysb.2004.04.024, [arXiv:hep-ph/0404111].

[30] M. Botje, “QCDNUM: Fast QCD Evolution and Convolution”, Comput. Phys. Commun. 182 (2011) 490, doi:10.1016/j.cpc.2010.10.020, [arXiv:1005.1481].

[31] F. D. Aaron *et al.* [H1 Collaboration], “Inclusive Deep Inelastic Scattering at High Q^2 with Longitudinally Polarised Lepton Beams at HERA, JHEP **09**, (2012) 061 doi:10.1007/JHEP09(2012)061 [arXiv:1206.7007 [hep-ex]].

[32] W. J. Stirling, R. S. Thorne and G. Watt, “Parton distributions for the LHC”, Eur. Phys. J C63 (2009) 189, doi: 10.1140/epjc/s10052-009-1072-5, [arXiv:0901.0002].

[33] W. T. Giele and S. Keller, “Implications of hadron collider observables on parton distribution function uncertainties,” Phys. Rev. D **58** (1998) 094023 doi:10.1103/PhysRevD.58.094023 [hep-ph/9803393].

[34] W. T. Giele, S. A. Keller and D. A. Kosower, “Parton distribution function uncertainties,” hep-ph/0104052.

[35] S. Alekhin, J. Blümlein and S. Moch, “Parton Distribution Functions and Benchmark Cross Sections at NNLO,” Phys. Rev. D **86** (2012) 054009 doi:10.1103/PhysRevD.86.054009 [arXiv:1202.2281 [hep-ph]].

[36] S. Alekhin, J. Blümlein, S. Moch and R. Placakyte, “Parton Distribution Functions, α_s and Heavy-Quark Masses for LHC Run II,” arXiv:1701.05838 [hep-ph].

Data set	Tagging	Q^2 range [GeV^2]	N_c	$\mathscr{L}$ [pb^{-1}]	$\sqrt{s}$ [GeV]	N_b
1 H1 VTX [8]	VTX	5 – 2000	29	245	318	12
2 H1 D^{*+} HERA-I [9]	D^{*+}	2 – 100	17	47	318	
3 H1 D^{*+} HERA-II (medium Q^2) [10]	D^{*+}	5 – 100	25	348	318	
4 H1 D^{*+} HERA-II (high Q^2) [11]	D^{*+}	100 – 1000	6	351	318	
5 ZEUS D^{*+} 96-97 [12]	D^{*+}	1 – 200	21	37	300	
6 ZEUS D^{*+} 98-00 [13]	D^{*+}	1.5 – 1000	31	82	318	
7 ZEUS D^0 2005 [14]	D^0	5 – 1000	9	134	318	
8 ZEUS μ 2005 [7]	μ	20 – 10000	8	126	318	8
9 ZEUS D^+ HERA-II [2]	D^+	5 – 1000	14	354	318	
10 ZEUS D^{*+} HERA-II [3]	D^{*+}	5 – 1000	31	363	318	
11 ZEUS VTX HERA-II [4]	VTX	5 – 1000	18	354	318	17
12 ZEUS e HERA-II [5]	e	10 – 1000		363	318	9
13 ZEUS μ + jet HERA-I [6]	μ	2 – 3000		114	318	11

Table 1: Data sets used in the combination. For each data set the Q^2 range, integrated luminosity ($\mathscr{L}$), centre-of-mass energy ($\sqrt{s}$) and the numbers of charm (N_c) and beauty (N_b) measurements are given.

Dataset	PDF	χ^2	χ^2 with PDF unc.
HERA 2012 c [1]	HERAPDF20_NLO_FF3A_EIG	59	59
	abm11_3n_nlo	62	62
(dof = 52)	ABMP16_3_nnlo	64	63
New combined c	HERAPDF20_NLO_FF3A_EIG	86	85
	abm11_3n_nlo	92	91
(dof = 52)	ABMP16_3_nnlo	101	99
ZEUS VTX b [4]	HERAPDF20_NLO_FF3A_EIG	14	14
	abm11_3n_nlo	13	13
(dof = 17)	ABMP16_3_nnlo	14	14
New combined b	HERAPDF20_NLO_FF3A_EIG	33	33
	abm11_3n_nlo	34	34
(dof = 27)	ABMP16_3_nnlo	39	39

Table 2: The χ^2 values and dof of the charm and beauty data with respect to the NLO and approximate NNLO calculations using various PDFs. The χ^2 values that include PDF uncertainties are shown separately.

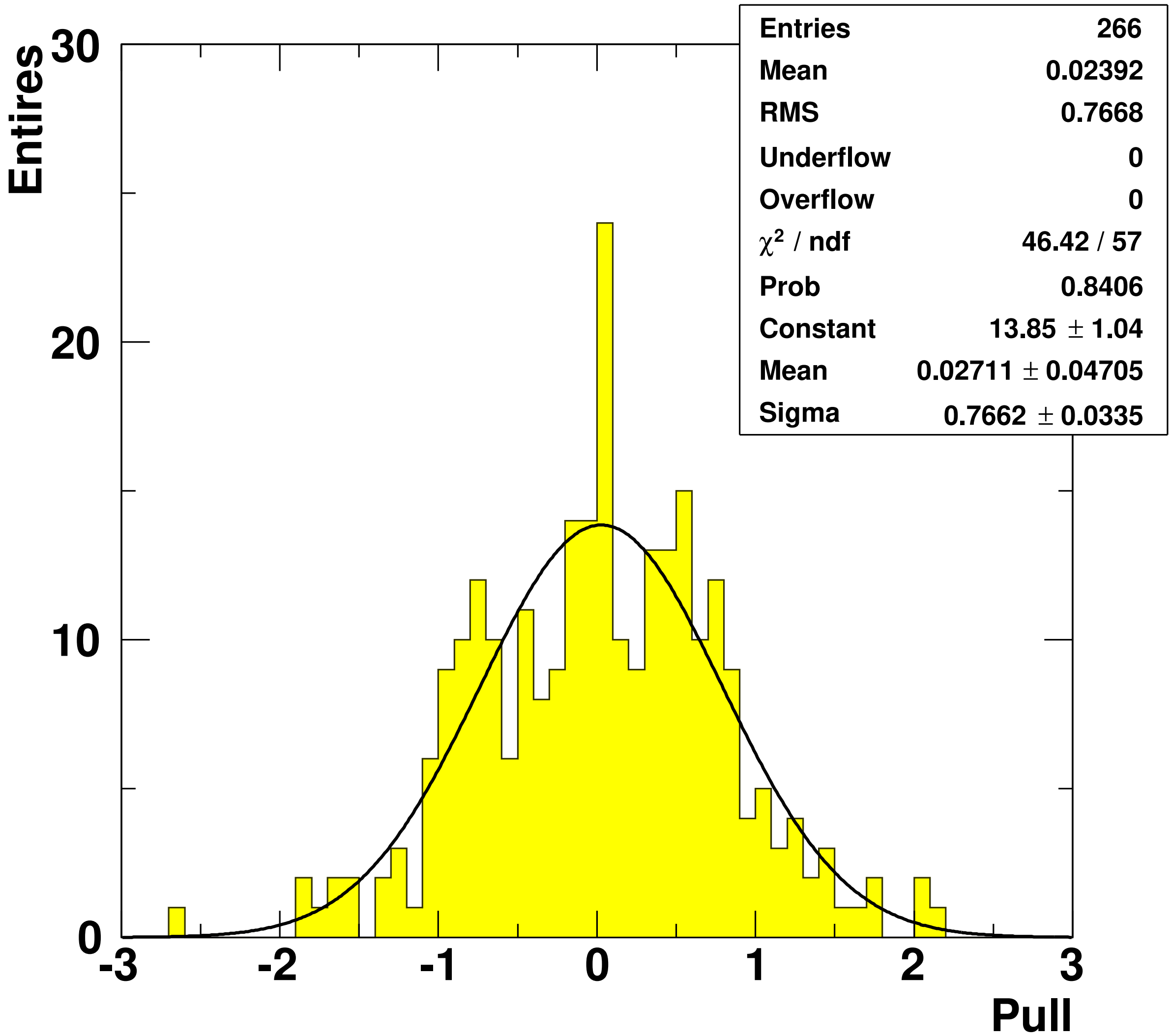

Figure 1: The pull distribution for the combination of the charm and beauty reduced cross sections.

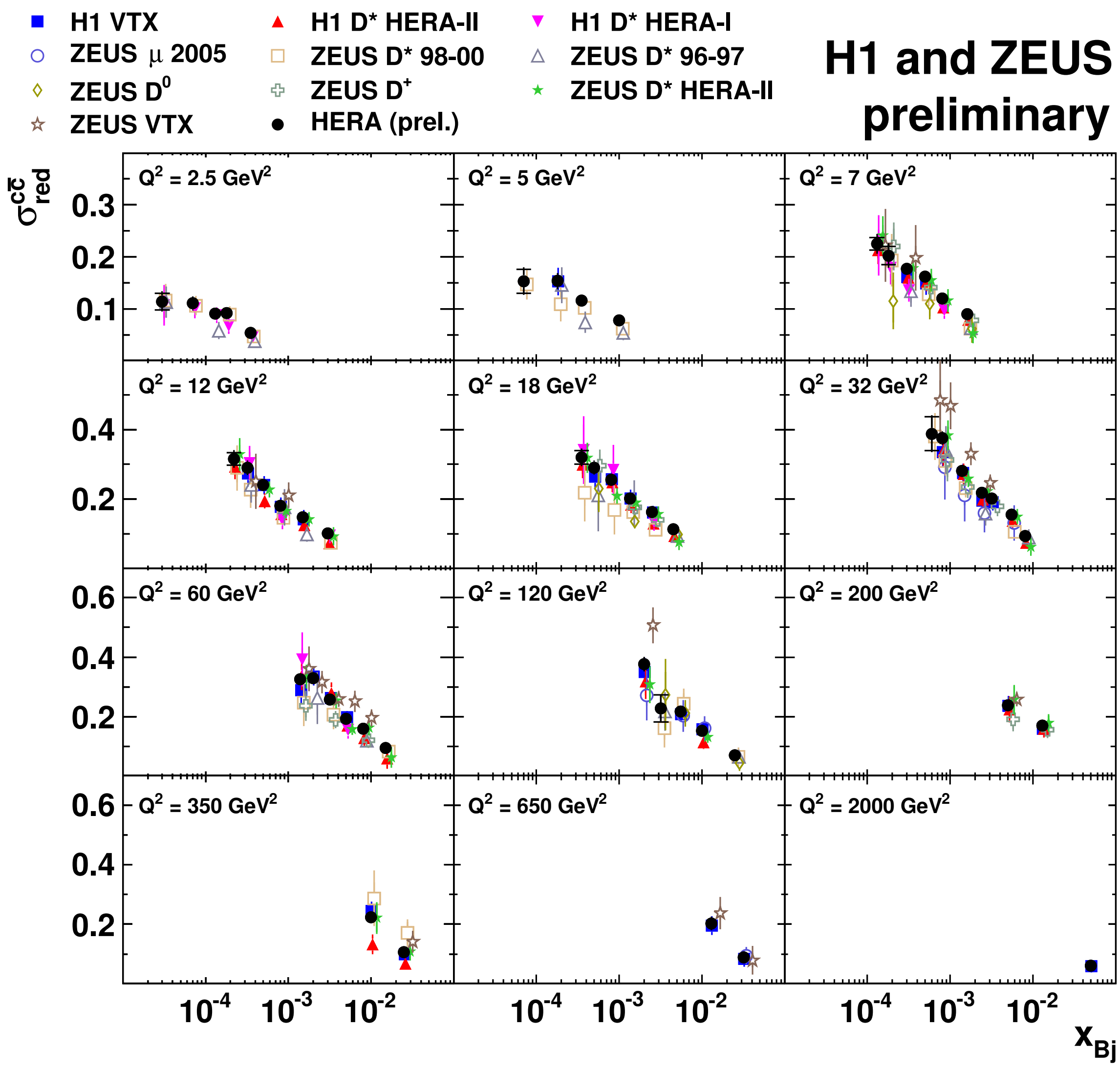

Figure 2: Combined measurements of the reduced charm production cross sections, $\sigma_{\rm red}^{c\bar{c}}$, (full circles) as a function of $x_{\rm Bj}$ for different values of Q^2. The inner error bars indicate the uncorrelated part of the uncertainties and the outer error bars represent the total uncertainties. The input measurements are also shown by the different markers. For presentation purposes each individual measurement is shifted in $x_{\rm Bj}$.

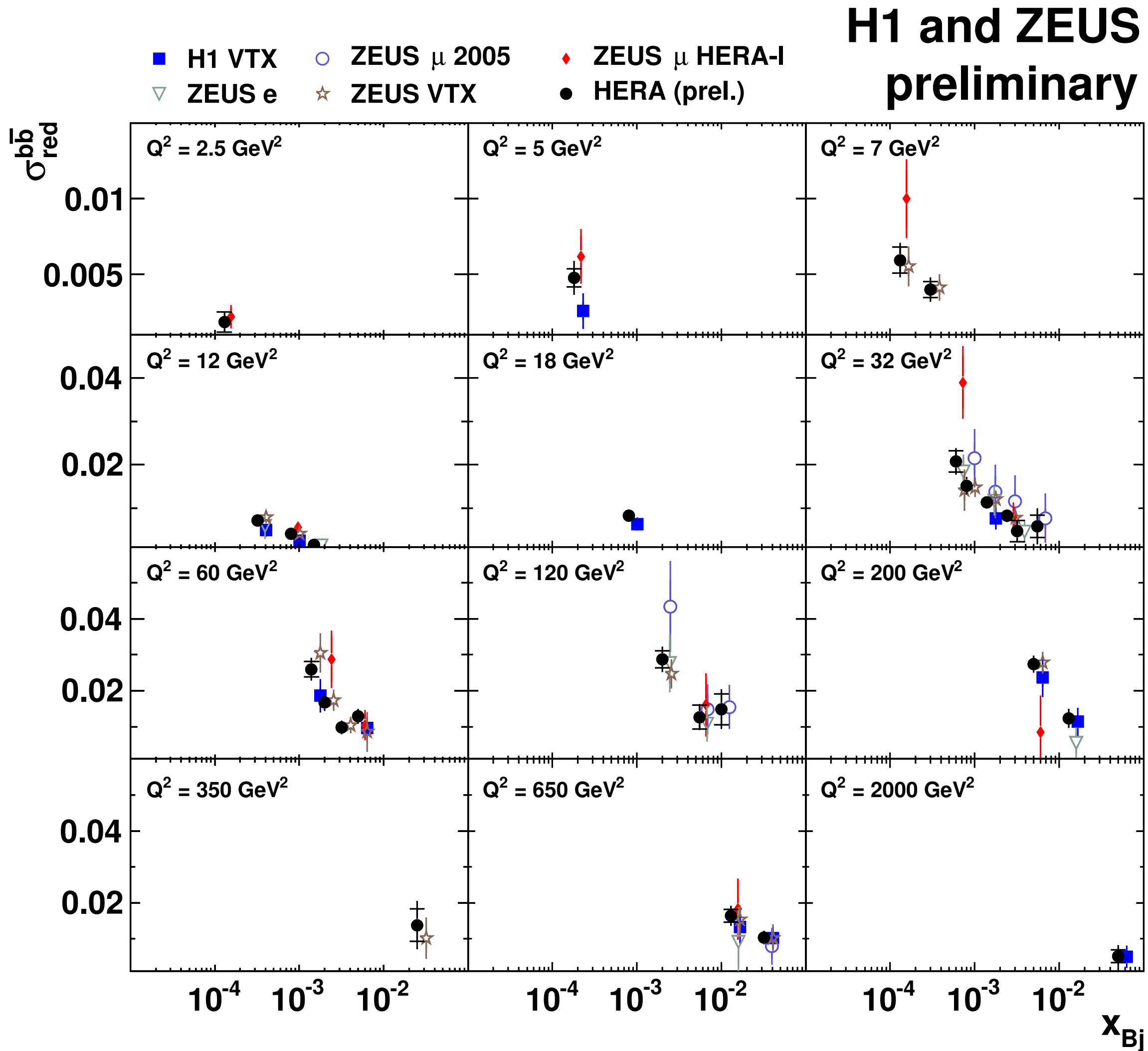

Figure 3: Combined measurements of the reduced beauty production cross sections, $\sigma_{\rm red}^{b\bar{b}}$, (full circles) as a function of $x_{\rm Bj}$ for different values of Q^2. The inner error bars indicate the uncorrelated part of the uncertainties and the outer error bars represent the total uncertainties. The input measurements are also shown by the different markers. For presentation purposes each individual measurement is shifted in $x_{\rm Bj}$.

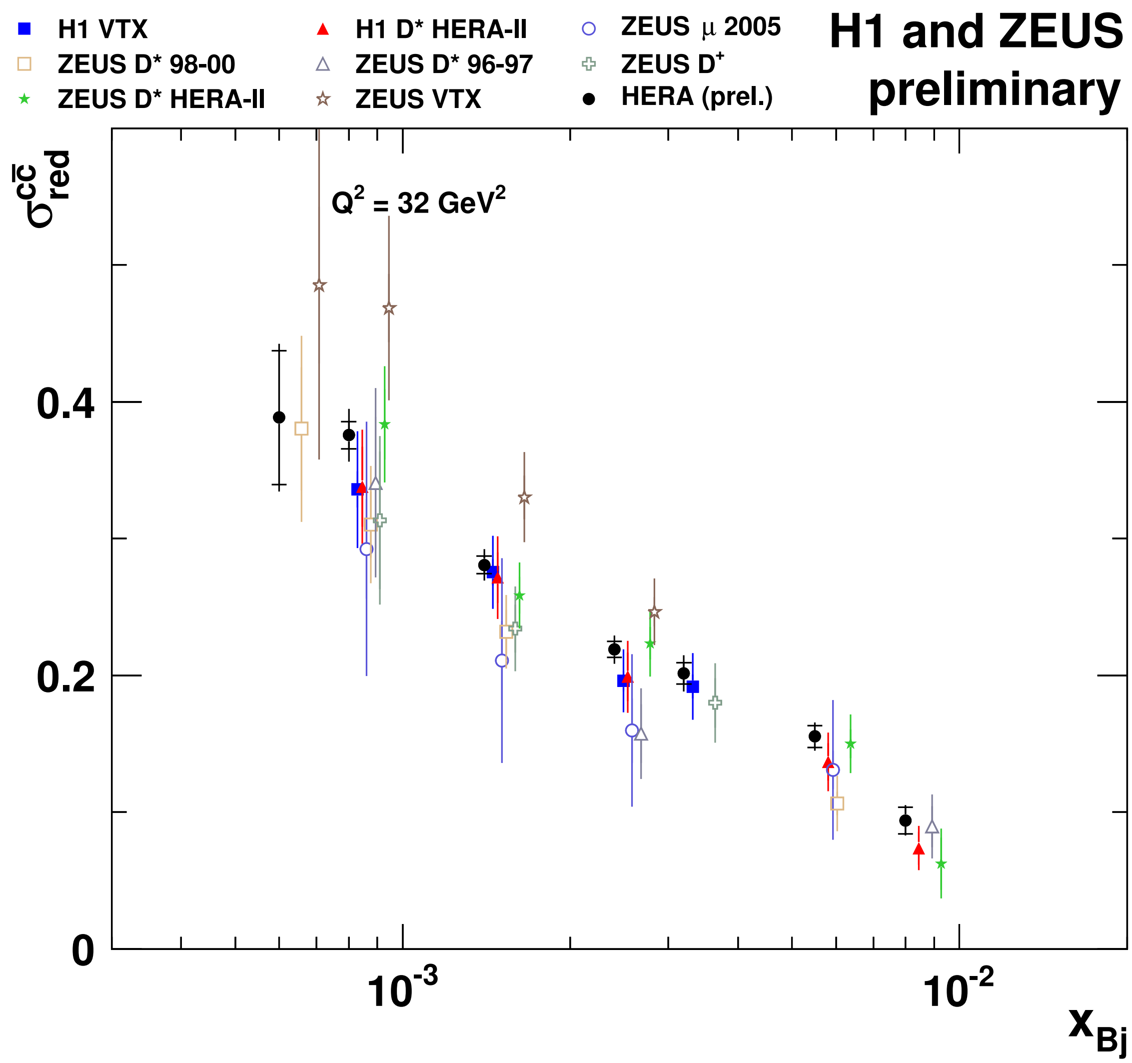

Figure 4: Combined measurements of the reduced charm production cross sections, $\sigma_{\rm red}^{c\bar{c}}$, (full circles) as a function of $x_{\rm Bj}$ for $Q^2 = 32$ GeV^2. The inner error bars indicate the uncorrelated part of the uncertainties and the outer error bars represent the total uncertainties. The input measurements are also shown by the different markers. For presentation purposes each individual measurement is shifted in $x_{\rm Bj}$.

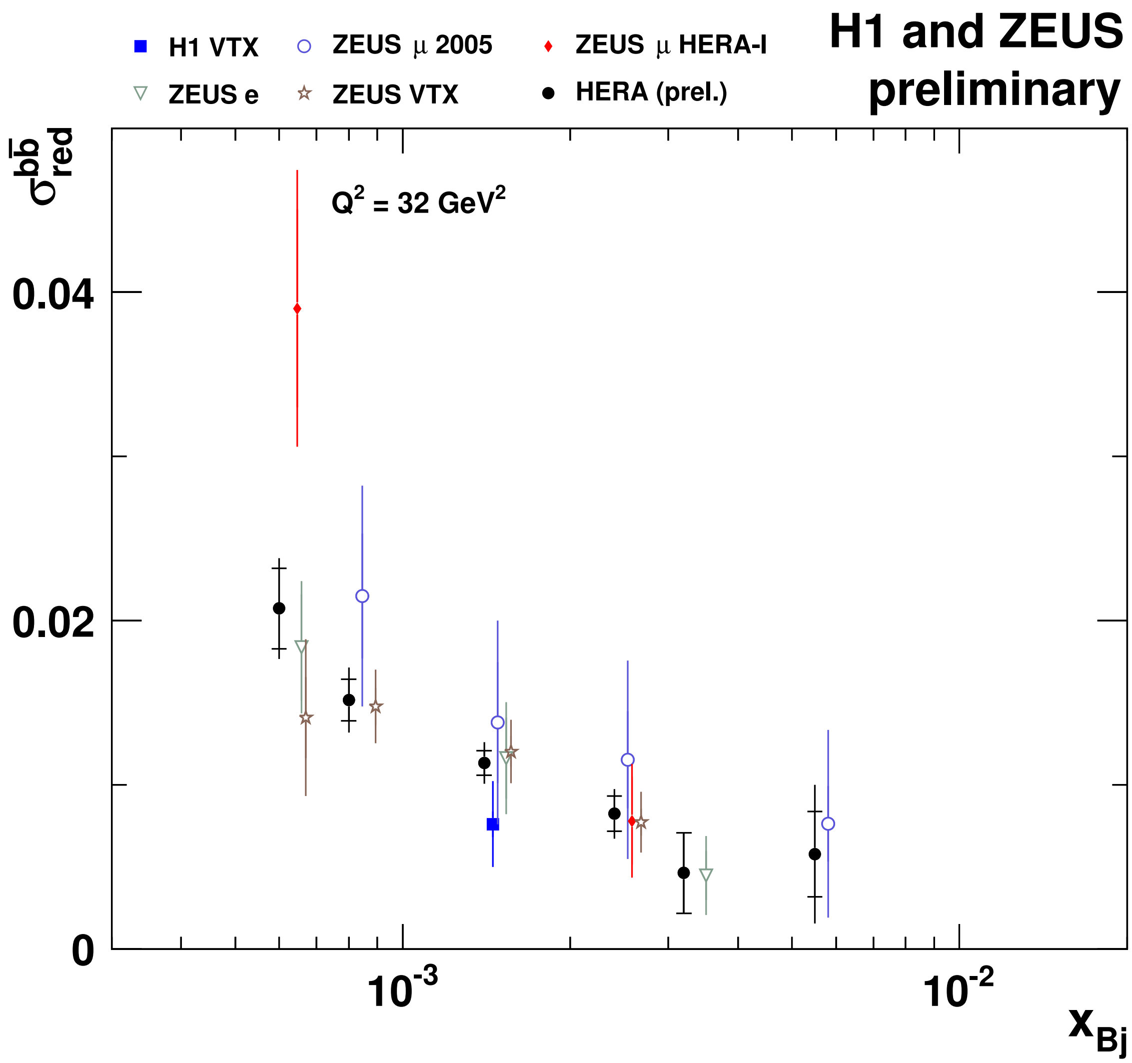

Figure 5: Combined measurements of the reduced beauty production cross sections, $\sigma_{\rm red}^{c\bar{c}}$, (full circles) as a function of $x_{\rm Bj}$ for $Q^2 = 32$ GeV^2. The inner error bars indicate the uncorrelated part of the uncertainties and the outer error bars represent the total uncertainties. The input measurements are also shown by the different markers. For presentation purposes each individual measurement is shifted in $x_{\rm Bj}$.

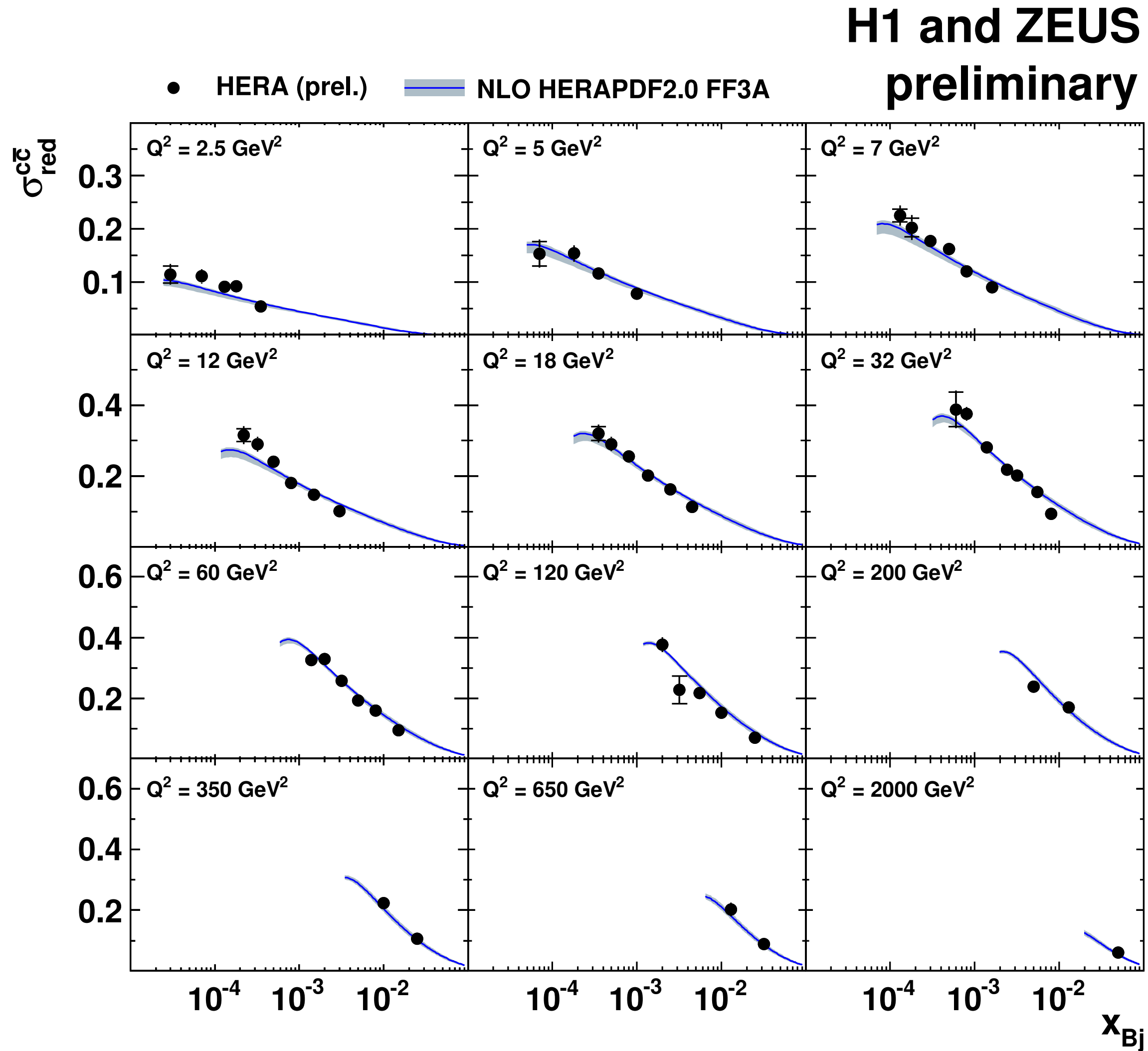

Figure 6: Combined reduced charm cross sections $\sigma_{\rm red}^{c\bar{c}}$ (full circles) as a function of $x_{\rm Bj}$ for given values of Q^2, compared to the NLO QCD theoretical predictions obtained using HERAPDF2.0 FF3A with their uncertainties (solid line with band).

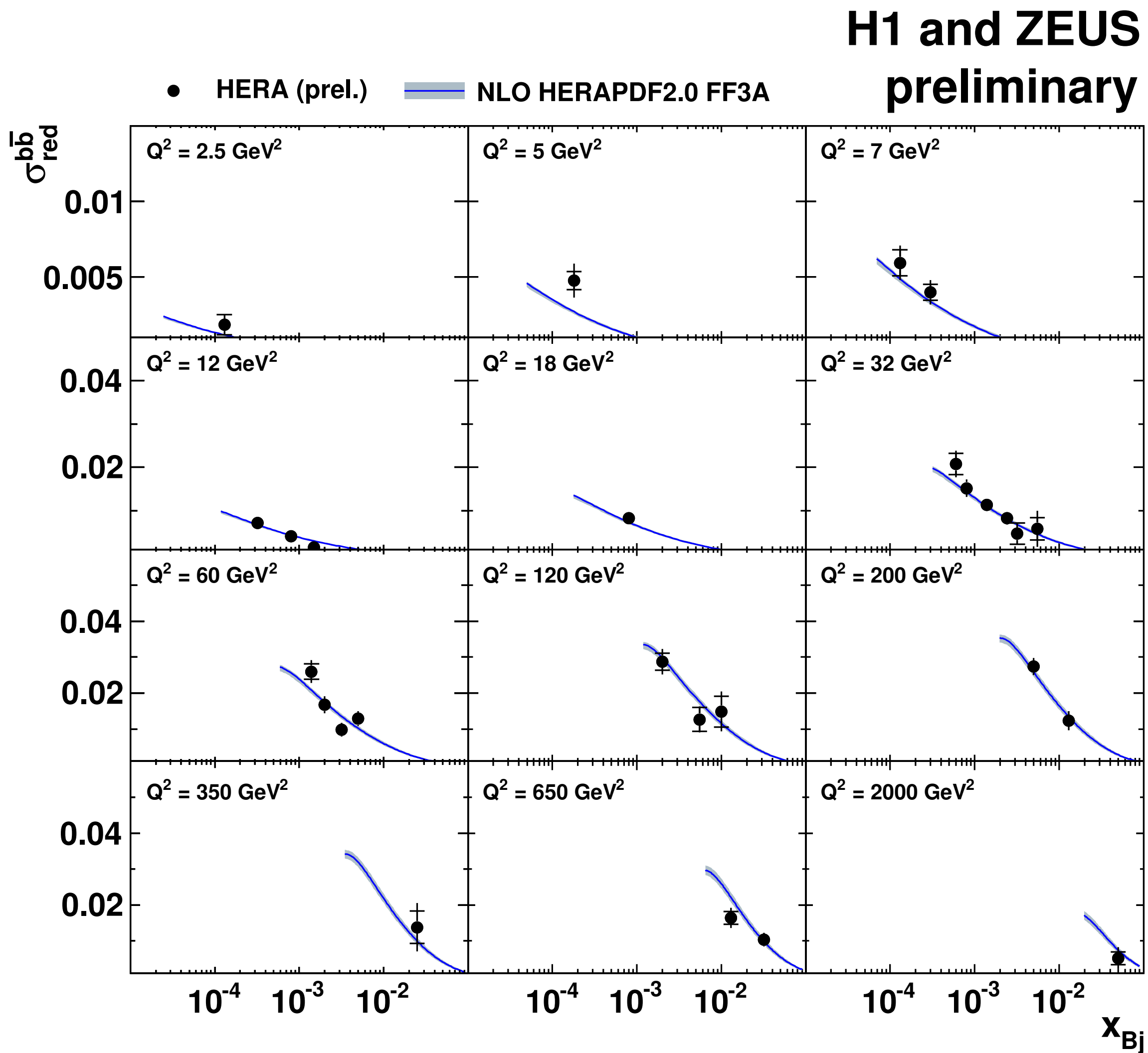

Figure 7: Combined reduced beauty cross sections $\sigma_{\rm red}^{b\bar{b}}$ (full circles) as a function of $x_{\rm Bj}$ for given values of Q^2, compared to the NLO QCD theoretical predictions obtained using HERA-PDF2.0 FF3A with their uncertainties (solid line with band).

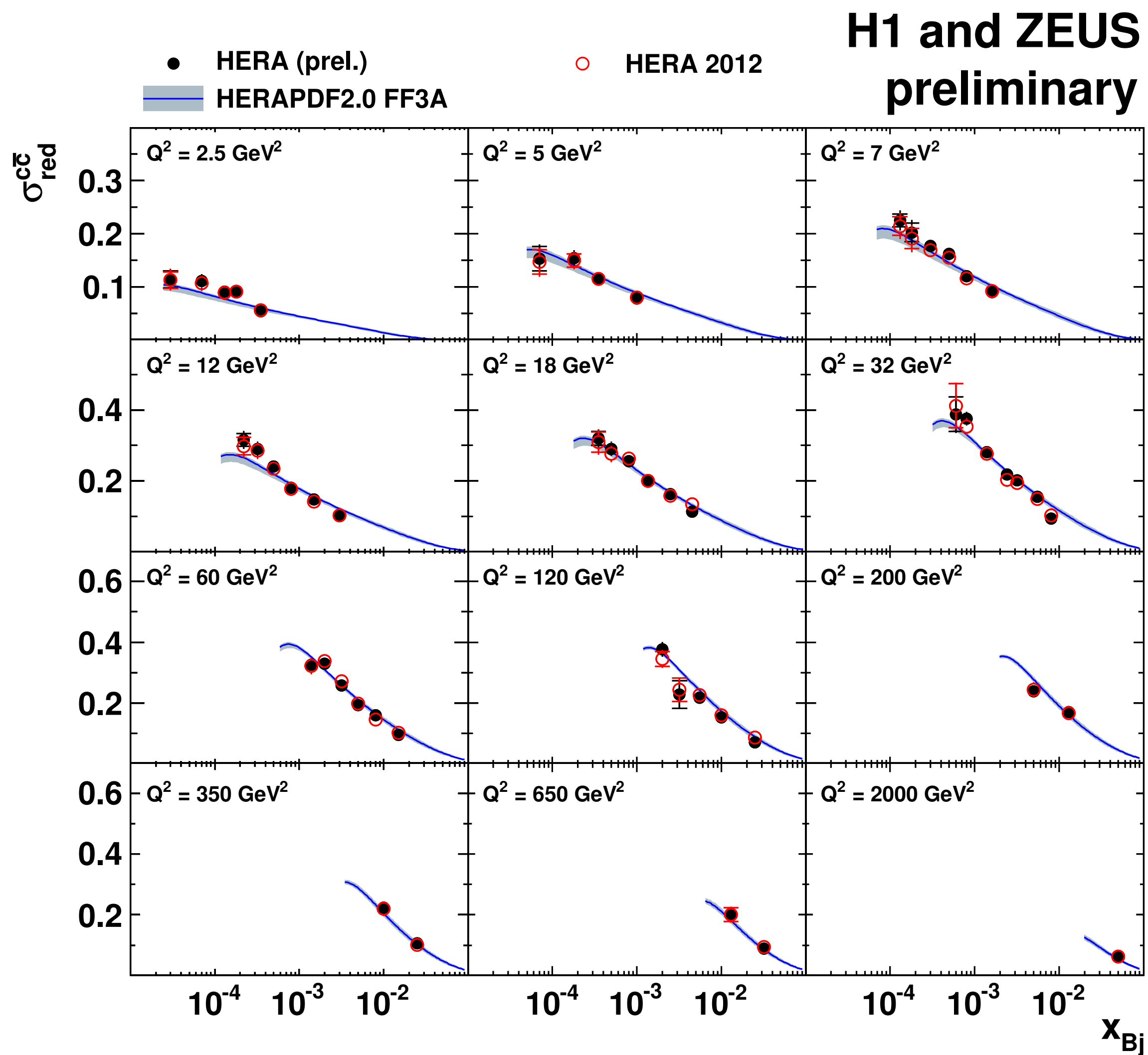

Figure 8: Combined reduced cross sections $\sigma_{\rm red}^{c\bar{c}}$ (full circles) as a function of $x_{\rm Bj}$ for given values of Q^2, compared to the results of the previous combination, denoted as 'HERA 2012' (open circles), and the NLO QCD theoretical predictions obtained using HERAPDF2.0 FF3A with their uncertainties (solid line with band).

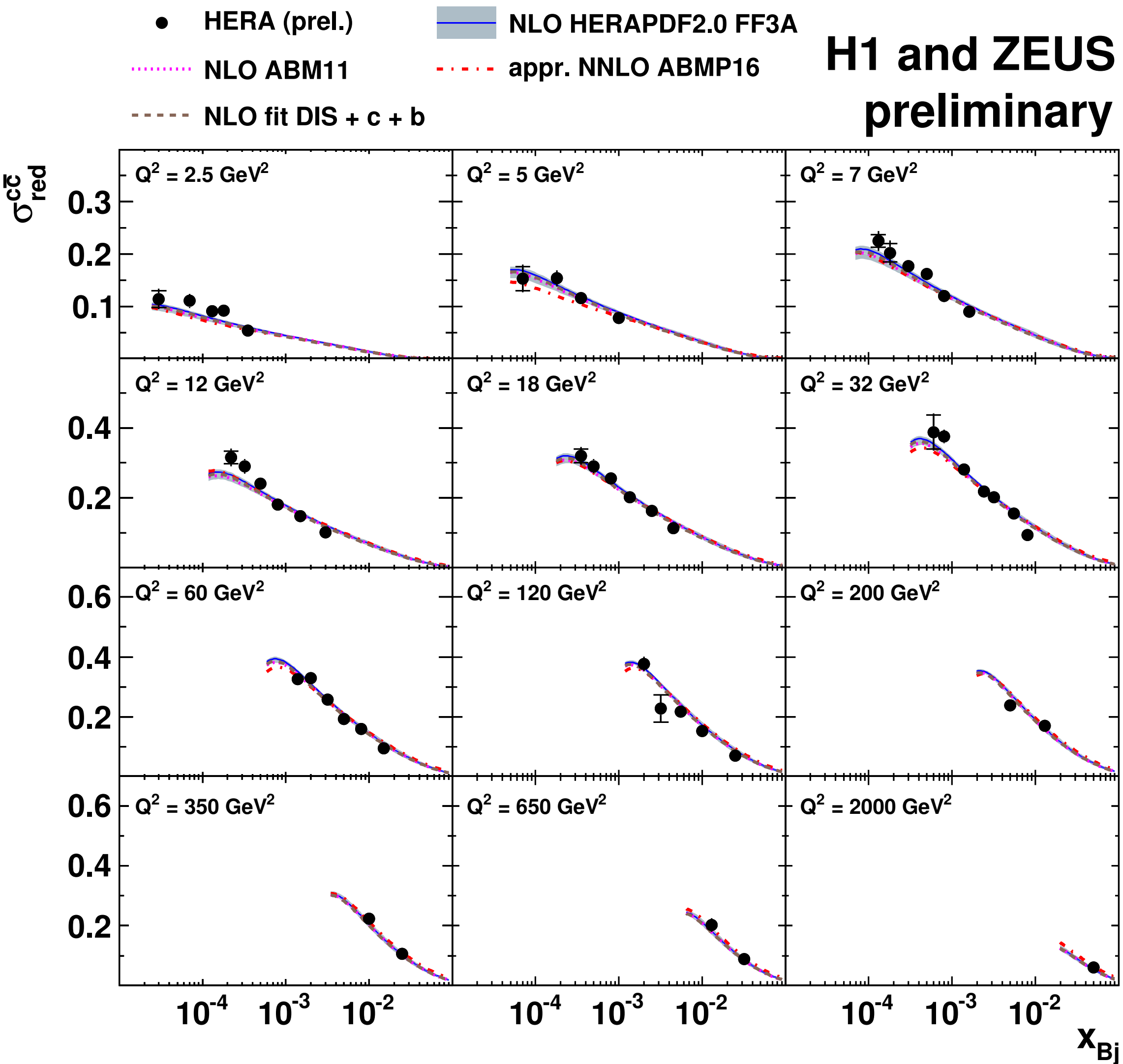

Figure 9: Combined reduced charm cross sections $\sigma_{\rm red}^{c\bar{c}}$ (full circles) as a function of $x_{\rm Bj}$ for given values of Q^2, compared to the NLO and approximate NNLO QCD theoretical predictions obtained using various PDFs.

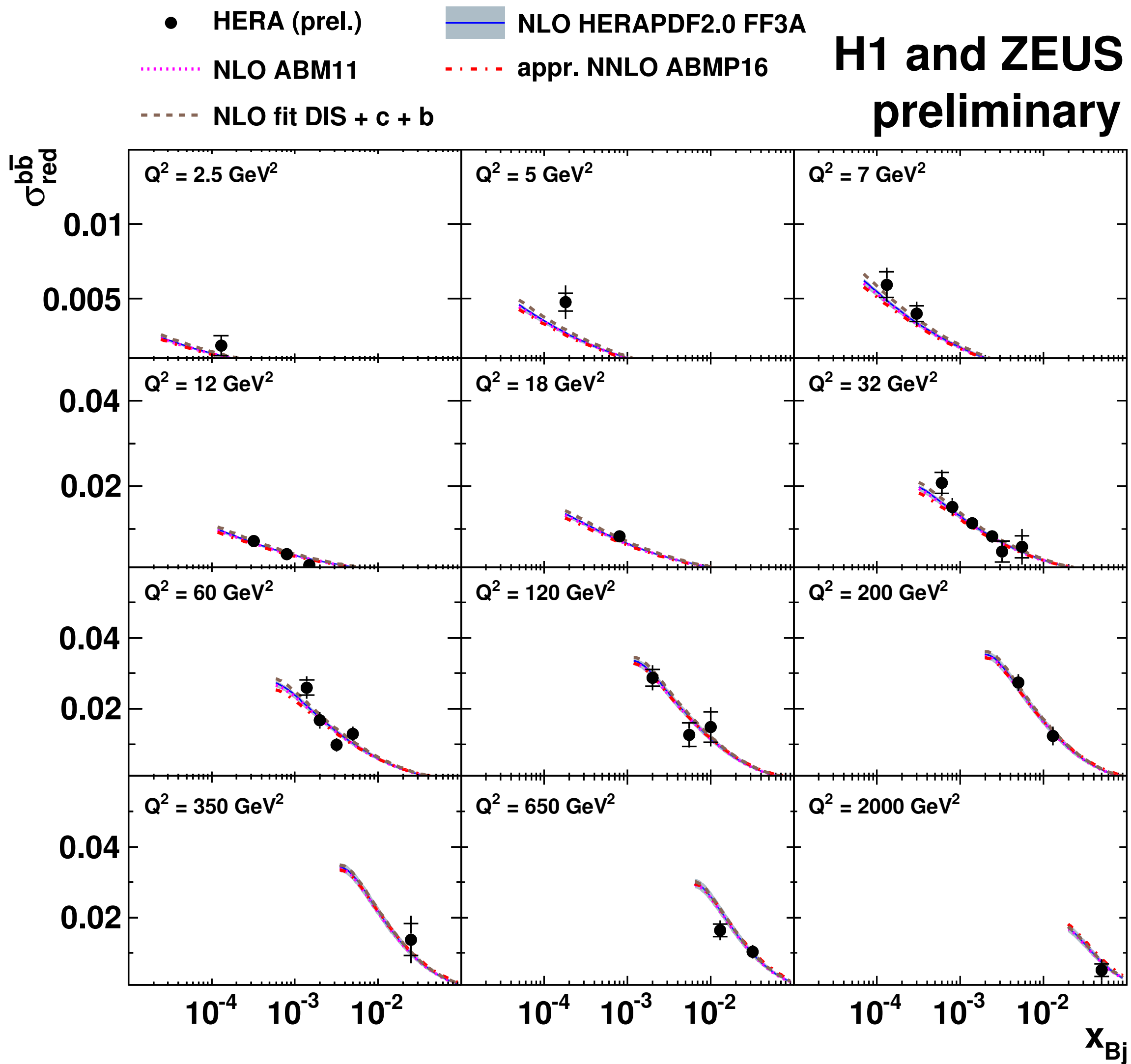

Figure 10: Combined reduced beauty cross sections $\sigma_{\text{red}}^{b\bar{b}}$ (full circles) as a function of x_{Bj} for given values of Q^2, compared to the NLO and approximate NNLO QCD theoretical predictions obtained using various PDFs.

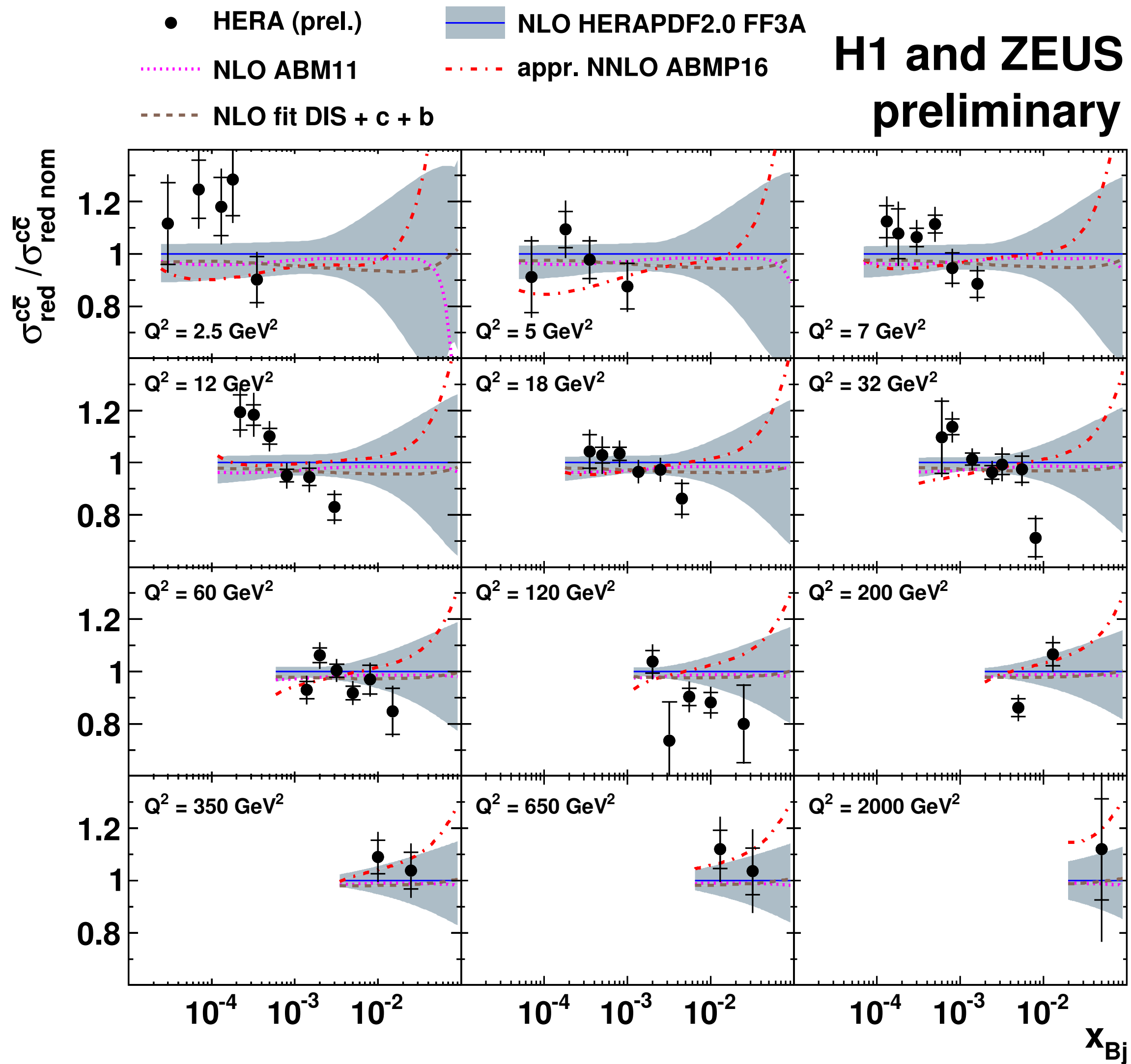

Figure 11: Combined reduced charm cross sections $\sigma_{\rm red}^{c\bar{c}}$ (full circles) as a function of $x_{\rm Bj}$ for given values of Q^2, compared to the NLO and approximate NNLO QCD theoretical predictions obtained using various PDFs, normalised to the predictions obtained using HERAPDF2.0 FF3A.

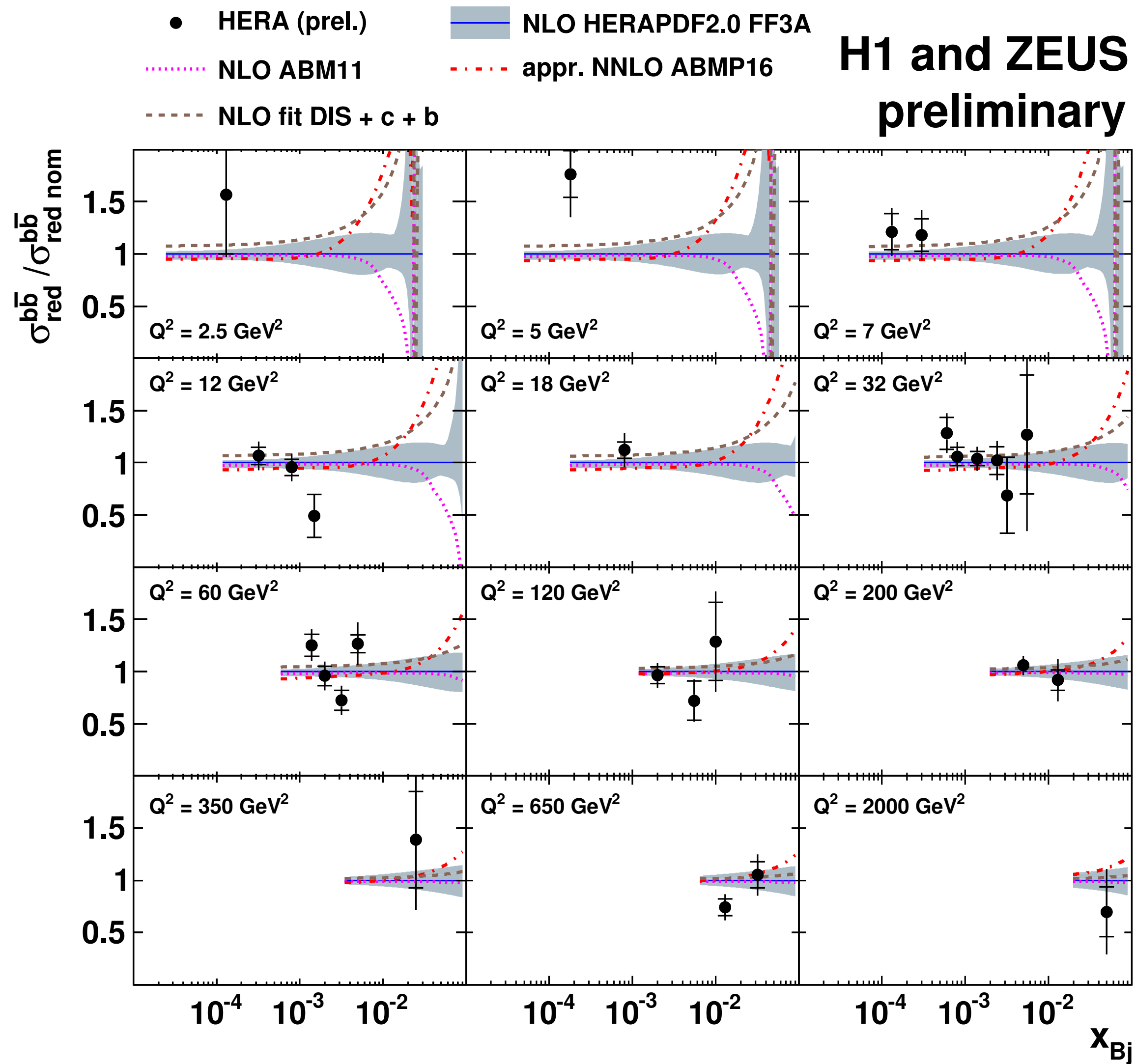

Figure 12: Combined reduced beauty cross sections $\sigma_{\rm red}^{b\bar{b}}$ (full circles) as a function of $x_{\rm Bj}$ for given values of Q^2, compared to the NLO and approximate NNLO QCD theoretical predictions obtained using various PDFs, normalised to the predictions obtained using HERAPDF2.0 FF3A.